THE JOURNAL OF PHYSICAL CHEMISTRY A
A JOURNAL OF THE AMERICAN CHEMICAL SOCIETY

pubs.acs.org/JPCA

Article

Rare Events Sampling Methods for Quantum and Classical Ab Initio Molecular Dynamics

Published as part of The Journal of Physical Chemistry A virtual special issue "Gregory A. Voth Festschrift".

Srinivasan S. Iyengar,* H. Bernhard Schlegel, Isaiah Sumner, and Junjie Li

Cite This: *J. Phys. Chem. A* 2024, 128, 5386−5397

Read Online

ACCESS | Metrics & More | Article Recommendations

ABSTRACT: We provide an approach to sample rare events during classical ab initio molecular dynamics and quantum wavepacket dynamics. For classical AIMD, a set of fictitious degrees of freedom are introduced that may harmonically interact with the electronic and nuclear degrees of freedom to steer the dynamics in a conservative fashion toward energetically forbidden regions. A similar approach when introduced for quantum wavepacket dynamics has the effect of biasing the trajectory of the wavepacket centroid toward the regions of the potential surface that are difficult to sample. The approach is demonstrated for a phenol-amine system, which is a prototypical problem for condensed phase-proton transfer, and for model potentials undergoing wavepacket dynamics. In all cases, the approach yields trajectories that conserve energy while sampling rare events.

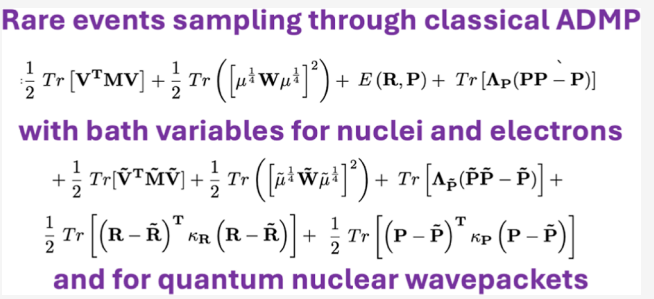

1. INTRODUCTION

Critical chemical processes occur over a range of time-scales spanning several orders of magnitude. For example, proton transfer in enzyme complexes may occur in the femto- to picosecond scale, which can be readily simulated using AIMD methods.[1−9] By contrast, larger-scale conformational transformations in proteins and biomolecules may occur over micro- to milli-seconds,[10,11] and are currently inaccessible to most molecular dynamics approaches. Such events are generally classified as "rare events."[11−35]

One approach for MD to sample these events would be to increase the rate of occurrence. Several methods have been implemented to overcome this issue.[11−24,26−41] A few of these methods are briefly reviewed here. In transition path sampling,[11,40] given a precomputed path that connects two potential energy wells, Chandler and co-workers use a Monte Carlo procedure with importance sampling based on the classical action, to find an ensemble of other productive trajectories (transition path ensemble). Other efforts along a similar vein are discussed in refs 12,15,22,23,36. In general, these methods attempt to variationally optimize the discrete classical action for paths connecting two points in configuration space.

Other schemes utilize fictitious degrees of freedom to bias a trajectory in a specific direction.[18,20,24,30−32,37,41] These methods all hinge on the assumption that if massive, fictitious degrees of freedom are tethered to nuclear degrees of freedom via some attractive potential, the fictitious particles can force the motion of the nuclei along a particular direction. These methods differ in how the dynamics of the fictitious particles are treated. In steered molecular dynamics (SMD),[24,32] the fictitious degrees of freedom are given a constant velocity. SMD is generally utilized to force the unfolding of proteins and mimic atomic force microscopy (AFM) experiments. In the scheme by Paci and Karplus,[41] the fictitious particles move with their respective nuclei and exert no force as long as the nuclei are moving in the "forward" direction along the reaction coordinate. However, the fictitious particles remain fixed and exert a force if the nuclei move backward. The remaining methodologies[18,20,37] allow the fictitious particles to follow classical trajectories and they differ in how these classical particles bias the molecular motion toward a specific goal. We also note that these methods are similar to extended Lagrangian formalisms[3,7,42−45] that have been used routinely to create distribution functions commensurate with other ensembles and also to obtain approximations to the dynamics of electrons and nuclei. For example, the Nose−Hoover[44,45] and Andersen thermostats[42] involve fictitious particles that

Received: November 7, 2023
Revised: May 29, 2024
Accepted: June 5, 2024
Published: July 1, 2024

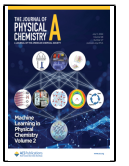

https://doi.org/10.1021/acs.jpca.3c07385
J. Phys. Chem. A 2024, 128, 5386−5397

enforce Lagrangian constraints as part of a super-Hamiltonian, which conserves the total energy; but the system Hamiltonian samples an NPT or *NVT* ensemble. Similar generalizations exist for grand-canonical ensembles as well.

Another common approach is to create biased ensembles[17,21,27,38] through biased initial conditions and biased potentials[26,39] to improve the likelihood of rare events. Although these algorithms are generally applied to classical MD, a notable exception is from Hammes-Schiffer and Tully,[27] who implemented their scheme in conjunction with their quantum-classical, surface hopping dynamics.[46]

Finally, rare events also have a significant role in creating free-energy surfaces from Jarzynski's equality (JE).[21,31,32,47−51] JE relates nonequilibrium work to the change in free energy by, $\exp\{-\beta\Delta F\} = \langle \exp\{-\beta W\}\rangle$, where $\beta \equiv 1/k_B T$ (k_B is Boltzmann's constant, T is temperature, W is nonequilibrium work, and $\langle\cdots\rangle$ indicates an ensemble average). Generally, to construct a free energy surface from this equality, a system is forced along a particular reaction coordinate and the work done over the reaction coordinate is calculated. Often, the methods listed above are implemented with the goal of generating free energy surfaces from JE.[21,31,32] However, the negative exponential dependence on work implies that the ensemble average is dominated by low work trajectories which rarely occur. Andricioaei and co-workers use their biased ensemble technique, Skew'm,[21]o attempt to address this problem. The authors do so by generating an ensemble of initial conditions that are biased toward a particular direction. For example, they can bias the ensemble to sample trajectories that require less work to force over barriers. They are then able to calculate the unbiased ensemble average.

In Sections 2 and 3, we outline our approach to address the problem of rare event sampling in both classical AIMD and quantum wavepacket based AIMD (QWAIMD).[52−59] Our classical AIMD results are presented in Section 4.2 and our QWAIMD results are discussed in Section 4.1. It must be noted that our approach is fully ab initio and hence has close connections to the studies proposed in ref 18. However, our approach is also strongly influenced by methods such as Steered Molecular Dynamics.[24,25] Conclusions are given in Section 5.

2. CLASSICAL AIMD METHODOLOGY INFLUENCED BY THE CALDEIRA−LEGGETT THEORY OF QUANTUM DISSIPATION

We introduce a Caldeira−Leggett-based[33−35,60,61] system-bath Hamiltonian for electron nuclear systems coupled to bath variables. This approach is similar to the fictitious particle methods discussed in the introduction. However, unlike in standard Langevin approaches,[42−45] our formalism has no random force, since the "bath" particles are explicitly propagated via a unique Hamiltonian.

We begin by introducing a Car−Parrinello-like[3] extended Hamiltonian with Lagrangian constraints that use atom-centered electronic basis functions and single particle density matrices. This is hence based on the atom centered density matrix (ADMP) formalism[7−9,62−65] and given by

$$\mathcal{H}_S = \frac{1}{2}\mathrm{Tr}[\mathbf{V}^T\mathbf{M}\mathbf{V}] + \frac{1}{2}\mathrm{Tr}([\mu^{1/4}\mathbf{W}\mu^{1/4}]^2) + E(\mathbf{R},\mathbf{P}) + \mathrm{Tr}[\mathbf{\Lambda_P}(\mathbf{P}\mathbf{P}-\mathbf{P})] \quad (1)$$

Here $\mathbf{M}$, $\mathbf{R}$, and $\mathbf{V}$ are the nuclear masses, positions, and velocities. Likewise, $\mathbf{P}$, $\mathbf{W}$, and μ are the single-particle electronic density matrix, density matrix velocity, and the fictitious inertia tensor,[8] respectively. The quantity $E(\mathbf{R},\mathbf{P})$ is the ab initio potential energy function obtained from a single-particle theory such as DFT. The last term in eq 1, imposes the so-called N-representability constraints on the single-particle density matrix, which amount to constraints on total number of electrons and on the idempotency of the density matrix using a Lagrangian multiplier matrix Λ_P. In refs 65−69, eq 1 has been generalized to include post-Hartree−Fock (CCSD) levels of theory, on-the-fly, thus providing a Car−Parrinello-like method with CCSD[65] and MP2[68] accuracy, along with on-the-fly basis set extrapolation.[69] It must be noted that eq 1 is purely classical Hamiltonian that governs the dynamics of parameters $\{\mathbf{P},\mathbf{W},\mathbf{R},\mathbf{V}\}$. In ref 70, a Bohmian mechanics[71−76] based generalization to eq 1 has been presented.

We now introduce (a) a family of nuclear bath variables, $\tilde{\mathbf{R}}$, with $\tilde{\mathbf{M}}$, $\tilde{\mathbf{R}}$, and $\tilde{\mathbf{V}}$ representing the masses, positions and velocities, and similarly (b) a set of electronic bath variables labeled as $\tilde{\mathbf{P}}$, with quantities $\tilde{\mu}$, $\tilde{\mathbf{P}}$, and $\tilde{\mathbf{W}}$ representing the bath density matrix inertia, density matrix and density matrix velocities. The quantity, $\tilde{\mathbf{P}}$, must have the same physical dimensions as $\mathbf{P}$. In extended Lagrangian formalisms like ADMP, $\mathbf{P}$ is a generalized classical variable, with inertia μ and velocity $\mathbf{W}$. Associated with this, the dynamics of $\tilde{\mathbf{P}}$, enforces a Lagrangian constraint that numerically biases $\mathbf{P}$, with inertia $\tilde{\mu}$, and velocity, $\tilde{\mathbf{W}}$, treated classically. When the bath variables are linearly coupled to the system variables, we obtain a system-bath Hamiltonian

$$\mathcal{H}_{SB} = \mathcal{H}_S + \frac{1}{2}\mathrm{Tr}[\tilde{\mathbf{V}}^T\tilde{\mathbf{M}}\tilde{\mathbf{V}}] + \frac{1}{2}\mathrm{Tr}([\tilde{\mu}^{1/4}\tilde{\mathbf{W}}\tilde{\mu}^{1/4}]^2) + \mathrm{Tr}[\mathbf{\Lambda}_{\tilde{\mathbf{P}}}(\tilde{\mathbf{P}}\tilde{\mathbf{P}}-\tilde{\mathbf{P}})] + \frac{1}{2}\mathrm{Tr}[(\mathbf{R}-\tilde{\mathbf{R}})^T\kappa_{\mathbf{R}}(\mathbf{R}-\tilde{\mathbf{R}})] + \frac{1}{2}\mathrm{Tr}[(\mathbf{P}-\tilde{\mathbf{P}})^T\kappa_{\mathbf{P}}(\mathbf{P}-\tilde{\mathbf{P}})] \quad (2)$$

where we have introduced the bath kinetic energies, $\frac{1}{2}\mathrm{Tr}[\tilde{\mathbf{V}}^T\tilde{\mathbf{M}}\tilde{\mathbf{V}}]$, and $\frac{1}{2}\mathrm{Tr}([\tilde{\mu}^{1/4}\tilde{\mathbf{W}}\tilde{\mu}^{1/4}]^2)$, and the system-bath coupling is captured by the last two terms. Specifically, the quantity, $\frac{1}{2}\mathrm{Tr}[(\mathbf{R}-\tilde{\mathbf{R}})^T\boldsymbol{\kappa}_{\mathbf{R}}(\mathbf{R}-\tilde{\mathbf{R}})]$, the harmonic potential constraining real variables to the "bath" variables used to drive the process".[60,61] Additionally, we have introduced the term, $\frac{1}{2}\mathrm{Tr}[(\mathbf{P}-\tilde{\mathbf{P}})^T\kappa_{\mathbf{P}}(\mathbf{P}-\tilde{\mathbf{P}})]$, which may be used to constrain the electronic density by introducing the variable, $\tilde{\mathbf{P}}$. Now, since $\tilde{\mathbf{P}}$ is dimensionally equivalent to $\mathbf{P}$, we include a similar N-representability term as in eq 1, that is, $\mathrm{Tr}[\mathbf{\Lambda}_{\tilde{\mathbf{P}}}(\tilde{\mathbf{P}}\tilde{\mathbf{P}}-\tilde{\mathbf{P}})]$. That is, an N-representable bath variable biases the dynamics of $\mathbf{P}$. The inclusion of these terms allow for a conservative Hamiltonian in eq 2, as can be seen from inspection of the total derivative of $\mathcal{H}_{SB}$ with respect to time in Appendix A, where we also provide a way to derive all equations of motion from eq 1. Additionally, these constraint terms may further be partitioned as per

https://doi.org/10.1021/acs.jpca.3c07385
J. Phys. Chem. A 2024, 128, 5386−5397

$$\frac{1}{2}\mathrm{Tr}[(\mathbf{R}-\tilde{\mathbf{R}})^{\mathrm{T}}\kappa_{\mathbf{R}}(\mathbf{R}-\tilde{\mathbf{R}})] = \frac{1}{2}\mathrm{Tr}[\tilde{\mathbf{R}}^{\mathrm{T}}\kappa_{\mathbf{R}}\tilde{\mathbf{R}}] - \mathrm{Tr}[\mathbf{R}^{\mathrm{T}}\kappa_{\mathbf{R}}\tilde{\mathbf{R}} + \tilde{\mathbf{R}}^{T}\kappa_{\mathbf{R}}\mathbf{R}] + \frac{1}{2}\mathrm{Tr}[\mathbf{R}^{\mathrm{T}}\kappa_{\mathbf{R}}\mathbf{R}] \tag{3}$$

and

$$\frac{1}{2}\mathrm{Tr}[(\mathbf{P}-\tilde{\mathbf{P}})^{\mathrm{T}}\kappa_{\mathbf{P}}(\mathbf{P}-\tilde{\mathbf{P}})] = \frac{1}{2}\mathrm{Tr}[\tilde{\mathbf{P}}^{\mathrm{T}}\kappa_{\mathbf{P}}\tilde{\mathbf{P}}] - \mathrm{Tr}[\mathbf{P}^{\mathrm{T}}\kappa_{\mathbf{P}}\tilde{\mathbf{P}} + \tilde{\mathbf{P}}^{T}\kappa_{\mathbf{P}}\mathbf{P}] + \frac{1}{2}\mathrm{Tr}[\mathbf{P}^{\mathrm{T}}\kappa_{\mathbf{P}}\mathbf{P}] \tag{4}$$

Here, $\kappa_{\mathbf{R}}$ and $\kappa_{\mathbf{P}}$ are the matrices that span the dimensionality of the electronic and nuclear basis spaces. Thus, there is potentially one set of bath variables to "drive" each system variable and as noted above, we have combined (a) the harmonic bath terms, $\frac{1}{2}\mathrm{Tr}[\tilde{\mathbf{R}}^{\mathrm{T}}\kappa_{\mathbf{R}}\tilde{\mathbf{R}}]$, and $\frac{1}{2}\mathrm{Tr}[\tilde{\mathbf{P}}^{\mathrm{T}}\kappa_{\mathbf{P}}\tilde{\mathbf{P}}]$, (b) the linear system-bath coupling terms, $\mathrm{Tr}[-\mathbf{R}^{\mathrm{T}}\kappa_{\mathbf{R}}\tilde{\mathbf{R}} - \tilde{\mathbf{R}}^{\mathrm{T}}\kappa_{\mathbf{R}}\mathbf{R}]$, and $\mathrm{Tr}[\mathbf{P}^{\mathrm{T}}\kappa_{\mathbf{P}}\tilde{\mathbf{P}} + \tilde{\mathbf{P}}^{\mathrm{T}}\kappa_{\mathbf{P}}\mathbf{P}]$ and (c) the harmonic potential constraining real variables to the "bath" variables used to drive the process",[60,61] $\frac{1}{2}\mathrm{Tr}[\mathbf{R}^{\mathrm{T}}\kappa_{\mathbf{R}}\mathbf{R}]$ and $\frac{1}{2}\mathrm{Tr}[\mathbf{P}^{\mathrm{T}}\kappa_{\mathbf{P}}\mathbf{P}]$ together into eq 2. Thus, the harmonic force-constants, $[\kappa_{\mathbf{R}};\kappa_{\mathbf{P}}]$, connect the system and bath variables. The quantities, $[\kappa_{\mathbf{R}};\kappa_{\mathbf{P}}]$, also determine the spectral density of the bath degrees of freedom. Equation 2 represents an ADMP generalization to system bath coupling using the Caldeira−Leggett theory.

We may also rewrite eq 2, using momenta which makes it convenient to connect to other methods. Thus

$$\begin{aligned}\mathcal{H}_{\mathrm{SB}} = {} & \frac{1}{2}\mathrm{Tr}[\mathcal{P}^{\mathrm{T}}\mathbf{M}^{-1}\mathcal{P}] + \frac{1}{2}\mathrm{Tr}([\mu^{-1/4}\mathcal{W}\mu^{-1/4}]^2) \\ & + \frac{1}{2}\mathrm{Tr}[\tilde{\mathcal{P}}^{\mathrm{T}}\tilde{\mathbf{M}}^{-1}\tilde{\mathcal{P}}] + \frac{1}{2}\mathrm{Tr}([\tilde{\mu}^{-1/4}\tilde{\mathcal{W}}\tilde{\mu}^{-1/4}]^2) \\ & + E(\mathbf{R},\mathbf{P}) + \mathrm{Tr}[\mathbf{\Lambda}_{\mathbf{P}}(\mathrm{PP}-\mathbf{P})] \\ & + \mathrm{Tr}[\mathbf{\Lambda}_{\tilde{\mathbf{P}}}(\tilde{\mathbf{P}}\tilde{\mathbf{P}}-\tilde{\mathbf{P}})] + \frac{1}{2}\mathrm{Tr}[(\mathbf{R}-\tilde{\mathbf{R}})^{\mathrm{T}}\kappa_{\mathbf{R}}(\mathbf{R}-\tilde{\mathbf{R}})] \\ & + \frac{1}{2}\mathrm{Tr}[(\mathbf{P}-\tilde{\mathbf{P}})^{\mathrm{T}}\kappa_{\mathbf{P}}(\mathbf{P}-\tilde{\mathbf{P}})]\end{aligned} \tag{5}$$

where $\tilde{\mathcal{P}}$, $\tilde{\mathcal{W}}$, $\tilde{\mathrm{M}}$, and $\tilde{\mu}$ are the momenta and mass tensors of the bath particles. From eq 5, we can derive the following equations of motion for the fictitious and molecular degrees of freedom, and this aspect is also discussed in Appendix A.

$$\begin{aligned}\frac{\mathrm{d}\mathcal{P}}{\mathrm{d}t} &= \{\mathcal{H}_{\mathrm{SB}},\mathcal{P}\} = -\nabla_{\mathbf{R}}\mathcal{H}_{\mathrm{SB}} \\ &= -\nabla_{\mathbf{R}}E(\mathbf{R},\mathbf{P}) \\ &\quad - \frac{1}{2}[\kappa_{\mathbf{R}}(\mathbf{R}-\tilde{\mathbf{R}}) + (\mathbf{R}-\tilde{\mathbf{R}})^{\mathrm{T}}\kappa_{\mathbf{R}}]\end{aligned} \tag{6}$$

$$\begin{aligned}\frac{\mathrm{d}\tilde{\mathcal{P}}}{\mathrm{d}t} &= \{\mathcal{H}_{\mathrm{SB}},\tilde{\mathcal{P}}\} = -\nabla_{\tilde{\mathbf{R}}}\mathcal{H}_{\mathrm{SB}} \\ &= \frac{1}{2}[\kappa_{\mathbf{R}}(\mathbf{R}-\tilde{\mathbf{R}}) + (\mathbf{R}-\tilde{\mathbf{R}})^{\mathrm{T}}\kappa_{\mathbf{R}}]\end{aligned} \tag{7}$$

$$\begin{aligned}\frac{\mathrm{d}\mathcal{W}}{\mathrm{d}t} &= \{\mathcal{H}_{\mathrm{SB}},\mathcal{W}\} = -\nabla_{\mathbf{P}}\mathcal{H}_{\mathrm{SB}} \\ &= -\nabla_{\mathbf{P}}E(\mathbf{R},\mathbf{P}) - [\mathbf{\Lambda}_{\mathbf{P}}\mathbf{P} + \mathbf{P}\mathbf{\Lambda}_{\mathbf{P}} - \mathbf{\Lambda}_{\mathbf{P}}] \\ &\quad - \frac{1}{2}[\kappa_{\mathbf{P}}(\mathbf{P}-\tilde{\mathbf{P}}) + (\mathbf{P}-\tilde{\mathbf{P}})^{\mathrm{T}}\kappa_{\mathbf{P}}]\end{aligned} \tag{8}$$

and

$$\begin{aligned}\frac{\mathrm{d}\tilde{\mathcal{W}}}{\mathrm{d}t} &= \{\mathcal{H}_{\mathrm{SB}},\tilde{\mathcal{W}}\} = -\nabla_{\tilde{\mathbf{P}}}\mathcal{H}_{\mathrm{SB}} \\ &= -[\mathbf{\Lambda}_{\tilde{\mathbf{P}}}\tilde{\mathbf{P}} + \tilde{\mathbf{P}}\mathbf{\Lambda}_{\tilde{\mathbf{P}}} - \mathbf{\Lambda}_{\tilde{\mathbf{P}}}] \\ &\quad + \frac{1}{2}[\kappa_{\mathbf{P}}(\mathbf{P}-\tilde{\mathbf{P}}) + (\mathbf{P}-\tilde{\mathbf{P}})^{\mathrm{T}}\kappa_{\mathbf{P}}]\end{aligned} \tag{9}$$

where {...} is a Poisson bracket.[77] The dynamics of the bath variables may therefore be utilized to bias specific nuclear and electronic degrees of freedom over potential barriers. In this way, our trajectories may be able access regions in phase space that are rarely sampled in nonbiased MD, such as product channels.

Equations 6, 7, 8, and 9 have an interesting connection to the generalized Langevin equation, which can be used to describe the dynamics of a system immersed in a bath of Brownian particles. The Langevin equation of motion for a system of particles can be written as

$$\frac{\mathrm{d}\mathcal{P}}{\mathrm{d}t} = -\nabla_{\mathbf{R}}V(\mathbf{R}) - \int_0^t \mathrm{d}\tau\mathcal{P}_\tau^{\mathrm{T}}\mathbf{M}^{-1}\xi_{t-\tau} + \varrho \tag{10}$$

where $\xi_{t-\tau}$ is a dynamic friction or memory kernel matrix with elements that depend on $t-\tau$ and ϱ is a "random" force. One may then connect this memory kernel to the formalism here, by collecting the terms in eqs 6 and 8 to obtain

$$\begin{aligned}&-\int_0^t \mathrm{d}\tau\mathcal{P}_\tau^{\mathrm{T}}\mathbf{M}^{-1}\xi_{t-\tau} + \varrho \\ &\rightarrow -\frac{1}{2}[\kappa_{\mathbf{R}}(\mathbf{R}-\tilde{\mathbf{R}}) + (\mathbf{R}-\tilde{\mathbf{R}})^{\mathrm{T}}\kappa_{\mathbf{R}}] \\ &\quad - [\mathbf{\Lambda}_{\tilde{\mathbf{P}}}\tilde{\mathbf{P}} + \tilde{\mathbf{P}}\mathbf{\Lambda}_{\tilde{\mathbf{P}}} - \mathbf{\Lambda}_{\tilde{\mathbf{P}}}] + \frac{1}{2}[\kappa_{\mathbf{P}}(\mathbf{P}-\tilde{\mathbf{P}}) \\ &\quad + (\mathbf{P}-\tilde{\mathbf{P}})^{\mathrm{T}}\kappa_{\mathbf{P}}]\end{aligned} \tag{11}$$

Thus, the "memory" here is generated by coupling to an external bath that drives the nuclear-electronic system degrees of freedom.

3. QUANTUM WAVEPACKET DYNAMICS WITH RARE EVENTS

In addition to classical treatment of rare events, there are several cases where quantum-mechanical treatment of nuclei is necessary,[52,55,56,78] and also may need a rare-events dynamics description. In this section we present a mixed-quantum-classical rare events sampling technique that is applied to the previously developed quantum wavepacket ab initio molecular dynamics (QWAIMD) approach.[52,56] In QWAIMD,[52−55,79] a general electron−nuclear system is partitioned into separate, but interacting parts:[80−83] subsystem 1 comprises nuclear degrees of freedom that are treated quantum dynamical manner. The degrees of freedom in subsystem 1 are represented by the variable R_{QM} below. Subsystem 2 contains nuclear degrees of freedom whose description will be given classically, and represented below using the symbol, $\mathbf{R}_{\mathbf{C}}$, and

https://doi.org/10.1021/acs.jpca.3c07385
J. Phys. Chem. A 2024, 128, 5386−5397

subsystem 3 comprises the electrons in the system. In our exposition here, unlike in the previous section, only the nuclear degrees of freedom (both classical and quantum) are exposed to a rare-events treatment. The resultant subsystem 1 description may follow Hamiltonian dynamics given by

$$\hat{H}_{\mathrm{I}} = \hat{K} + V(\mathbf{R_C}, R_{\mathrm{QM}}) + \frac{1}{2}\kappa_{\mathrm{QM}}(R_{\mathrm{QM}} - \tilde{R}_{\mathrm{QM}})^2 \tag{12}$$

where $\hat{K} \equiv -\frac{\hbar^2}{2M_{\mathrm{QM}}}\nabla^2_{R_{\mathrm{QM}}}$ is the kinetic energy operator and $\tilde{R}_{\mathrm{QM}}$ are fictitious degrees of freedom coupled to the quantum nuclear degrees of freedom, R_{QM}, with force constants κ_{QM}. The quantity, $V(\mathbf{R_C},R_{\mathrm{QM}})$ is the electronic potential energy surface, obtained as a function classical nuclear, $\mathbf{R_C}$ and quantum nuclear degrees of freedom. Correspondingly, the classical nuclear evolution may be derived from

$$\mathcal{H}_{\mathrm{II}} = \frac{1}{2}\mathrm{Tr}[\mathcal{P}_{\mathbf{C}}^{\mathbf{T}}\mathbf{M}^{-1}\mathcal{P}_{\mathbf{C}}] + \frac{1}{2}\mathrm{Tr}[\tilde{\mathcal{P}}_{\mathbf{C}}^{\mathbf{T}}\tilde{\mathbf{M}}^{-1}\tilde{\mathcal{P}}_{\mathbf{C}}] + \langle\chi|\hat{H}_{\mathrm{I}}|\chi\rangle + \frac{1}{2}\mathrm{Tr}[(\mathbf{R_C} - \tilde{\mathbf{R}}_{\mathbf{C}})^{\mathbf{T}}\kappa_{\mathbf{R}}(\mathbf{R_C} - \tilde{\mathbf{R}}_{\mathbf{C}})] \tag{13}$$

where we have introduce a wavepacket, $|\chi(R_{\mathrm{QM}})\rangle$, averaged interaction term: $\langle\chi|\hat{H}_{\mathrm{I}}|\chi\rangle$. From these Hamiltonians, we may derive the following equations of motion

$$\imath\hbar\frac{\partial}{\partial t}\chi(R_{\mathrm{QM}}; t) = \hat{H}_{\mathrm{I}}\chi(R_{\mathrm{QM}}; t) \tag{14}$$

$$\frac{\mathrm{d}\mathcal{P}_{\mathbf{C}}}{\mathrm{d}t} = -\langle\chi|\nabla_{\mathbf{R}_{\mathbf{C}}}V(\mathbf{R_C}, R_{\mathrm{QM}})|\chi\rangle - \frac{1}{2}[\kappa_{\mathbf{R}}(\mathbf{R_C} - \tilde{\mathbf{R}}_{\mathbf{C}}) + (\mathbf{R_C} - \tilde{\mathbf{R}}_{\mathbf{C}})^{\mathrm{T}}\kappa_{\mathbf{R}}] \tag{15}$$

$$\frac{\mathrm{d}\tilde{\mathcal{P}}_{\mathbf{C}}}{\mathrm{d}t} = \frac{1}{2}[\kappa_{\mathbf{R}}(\mathbf{R_C} - \tilde{\mathbf{R}}_{\mathbf{C}}) + (\mathbf{R_C} - \tilde{\mathbf{R}}_{\mathbf{C}})^{\mathrm{T}}\kappa_{\mathbf{R}}] \tag{16}$$

and

$$\frac{\mathrm{d}\tilde{\mathcal{P}}_{\mathrm{QM}}}{\mathrm{d}t} = \kappa_{\mathrm{QM}}(\langle\chi|R_{\mathrm{QM}}|\chi\rangle - \tilde{R}_{\mathrm{QM}}) \tag{17}$$

where, $\tilde{P}_{\mathrm{C}}$ is dictated by the choice of a mass parameter, $\tilde{M}_{\mathrm{C}}$, $\tilde{P}_{\mathrm{QM}}$ is dictated by the choice of a mass parameter, $\tilde{M}_{\mathrm{QM}}$, and these along with the respective force constants, $\kappa_{\mathbf{R}}$ and κ_{QM} together dictate the rate at which rare events sampling can be achived, while suitably sampling orthogonal degrees of freedom. The mass, $\tilde{M}_{\mathrm{QM}}$, has an impact on the momentum of the fictitious particle which provides one handle on how quickly or slowly the rare event sampling is meant to be conducted. On the contrary, the values of κ_{QM} and $\kappa_{\mathbf{R}}$ influence the extent to which the orthogonal degrees of freedom are sampled. For example, for small values of $\tilde{M}_{\mathrm{QM}}$, the fictitious mass may have a higher velocity at a given temperature. However, even in this case, by reducing κ_{QM} and $\kappa_{\mathbf{R}}$, sampling of orthogonal degrees of freedom can be achieved. By contrast at large values of $\tilde{M}_{\mathrm{QM}}$, the fictitious degree of freedom may have a lower momentum at a given temperature and here again suitable values of κ_{QM} and $\kappa_{\mathbf{R}}$ may allow appropriate sampling of orthogonal degrees of freedom. Therefore, in the results section, we first study the quantum dynamical sampling approach by fixing $\tilde{M}_{\mathrm{QM}}$ while varying κ_{QM}.

Additionally, eqs 12−17 contain three components: electronic degrees of freedom that yield the potential energy surface, $V(\mathbf{R_C},R_{\mathrm{QM}})$, quantum nuclear degrees of freedom, R_{QM}, and classical nuclear degrees of freedom, $\mathbf{R_C}$, along with associated bath variables. The electronic and quantum nuclear components are together represented within eq 12 (and attempts to generalize these have been discussed in refs 57 and 58), whereas the classical nuclear degrees of freedom are contained within eq 13. Nonadiabatic effects between the quantum nuclear and electronic degrees of freedom may be included by generalizing eq 12 as in refs 57 and 58, but these will involve approximations to multiple electronic surfaces and nonadiabatic couplings.[84−91] Additionally, when nonadiabatic effects between the classical nuclear and quantum nuclear degrees of freedom are needed (to improve correlation between these treatments), this necessitates generalizations of eqs 13 and 14 to a surface hopping[92,93] paradigm. However, these elaborate ideas are left for discussion in a future publication.

Toward integrating the above-mentioned equations of motion, given the time dependence of the potential in eq 14, arising from the constraint term: $\frac{1}{2}\kappa_{\mathrm{QM}}(R_{\mathrm{QM}} - \tilde{R}_{\mathrm{QM}})^2$, the propagation of eq 14 needs special handling? We thus approximate the time-dependence of the constraint potential by expanding this as a Taylor series

$$\begin{aligned} V_{\mathrm{C}}(R_{\mathrm{QM}}, \tilde{R}_{\mathrm{QM}}, t + \Delta t) &= \frac{1}{2}\kappa_{\mathrm{QM}}(R_{\mathrm{QM}} - \tilde{R}_{\mathrm{QM}})^2 \\ &\approx V_{\mathrm{C}}(R_{\mathrm{QM}}, \tilde{R}_{\mathrm{QM}}, t) + \left.\frac{\mathrm{d}V_{\mathrm{C}}(R_{\mathrm{QM}}, \tilde{R}_{\mathrm{QM}}, t)}{\mathrm{d}t}\right|_{t=t}\Delta t + \ldots \end{aligned} \tag{18}$$

and choose

$$\frac{\mathrm{d}V_{\mathrm{C}}(R_{\mathrm{QM}}, \tilde{R}_{\mathrm{QM}}, t)}{\mathrm{d}t} = \frac{\partial V_{\mathrm{C}}(R_{\mathrm{QM}}, \tilde{R}_{\mathrm{QM}}, t)}{\partial\tilde{R}_{\mathrm{QM}}}\frac{\partial\tilde{R}_{\mathrm{QM}}}{\partial t} \tag{19}$$

We then use this time-dependent potential in eq 14, which integrates to

$$\chi(R_{\mathrm{QM}}, \Delta t) = \mathcal{T}\left[\exp\left\{\frac{-1}{\hbar}\int_0^t \mathrm{d}t'\hat{H}_{\mathrm{I}}\right\}\right]\chi(R_{\mathrm{QM}}, t = 0) \tag{20}$$

where $\mathcal{T}$ is the time-order operator. Equation 20 is solved by invoking the Magnus expansion,[94] which we also truncate at first order so that eq 20 becomes

$$\chi(R_{\mathrm{QM}}, t + \Delta t) = \exp\left\{\frac{-1}{\hbar}\left(\hat{H}_{\mathrm{I}}\Delta t + \frac{1}{2}\frac{\partial V_{\mathrm{C}}}{\partial\tilde{R}_{\mathrm{QM}}}\frac{\partial\tilde{R}_{\mathrm{QM}}}{\partial t}\right|_{t=t}\Delta t^2\right)\right\} \times \chi(R_{\mathrm{QM}}, t) \tag{21}$$

4. NUMERICAL RESULTS FOR BIASED QUANTUM AND CLASSICAL TRAJECTORIES

In Section 4.1 we present numerical results for the quantum dynamical implementation of rare events sampling. This is done on model potentials. We then proceed in Section 4.2 to study biased AIMD trajectories for a phenol-amine system that

https://doi.org/10.1021/acs.jpca.3c07385
J. Phys. Chem. A 2024, 128, 5386−5397

has been considered prototypical for condensed phase proton transfer. For the system in Section 4.2, electronic variables are included as within classical ADMP without using $\tilde{\mathbf{P}}$ and $\tilde{\mathbf{W}}$. Equations 6−8 determine the dynamics in Section 4.2. In Section 4.1 electronic variables are not included in the dynamics and a potential energy surface is used, as can be seen from eqs 12 and 14. Equations 14 and 17 determine the dynamics in Section 4.1. On a related note, the methods in this paper aim to discover new rare events pathways during quantum and classical trajectory calculations. An example of how such a method can be useful is seen from refs 34 and 35, where a new hydrogen bond between isoleucine-839 and the substrate hydroxy group in the active side within the enzyme, soybean lipoxygenase-1, was discovered using a special case of the classical ADMP version of the method described here. It turns out that this new hydrogen bond changes the electric field inside the active side and could be an additional reason for the accelerated transfer process seen in soybean lipoxygenase-1. These aspects are not discussed here, and will be further evaluated in future publications using the wavepacket version discussed here.

4.1. Biased Quantum Wavepacket Dynamics on Model Systems. There are two kinds of analytical potentials that are used to benchmark our quantum rare events formalism. The first example (labeled system 1) is a simple quadratic potential, $V(\mathbf{R}_C, R_{QM}) \equiv \frac{1}{2}\kappa R_{QM}^2$, in eq 12, and thus the overall (biasing) potential has the form

$$\frac{1}{2}\kappa R_{QM}^2 + \frac{1}{2}\kappa_{QM}(R_{QM} - \tilde{R}_{QM})^2 \tag{22}$$

For the second systems (labeled system 2), $V(\mathbf{R}_C,R_{QM})$ is chosen as a double well potential function of R_{QM} with a barrier height of approximately 7.5 kcal/mol and a well-to-well distance of about 0.85 Å. Both of these models have been studied by other investigators within the context of quantum-classical dynamics.[95]

System 1: Since system 1 is fully harmonic, the dynamics of the wavepacket centroid and the fictitious (biasing) degree of freedom can be analytically solved via normal mode decomposition.[95] As discussed in Section 3, proper tuning of κ_{QM} should be sufficient to accommodate fictitious mass of different scale for appropriate sampling. Here we choose to fix $\tilde{M}_{QM}$ (see eq 17) and vary the value of κ_{QM} to demonstrate the impact of κ_{QM} on the dynamics. The fictitious mass is chosen to be $\tilde{M}_{QM} = 350$ amu, the initial kinetic energy of the fictitious particle is chosen to be 3.0 kcal/mol. The grid is comprised of 151 points spaced at 0.013 Å. In Figure 1a, we compare the propagation error for the wavepacket centroid as a function of the constraint force constant, κ_{QM} (see eq 12), for the zeroth-order propagation scheme (zeroth order Taylor expansion in eq 18) and the time-dependent scheme discussed in section. Three (first-order approximation). The error in numerical propagation is gauged by comparison with the analytical result by using the expression

$$\sigma_{prop} = \frac{1}{T}\int_0^T \left\| x_{ref}(t) - x_{prop}(t) \right\|_2 \mathrm{d}t \tag{23}$$

The quantity $\|\cdots\|_2$ is the L^2 norm,[96,97] T is the total propagation time and x_{ref} denotes the analytical form of the wavepacket or its centroid, whereas x_{prop} denotes the numerically propagated wavepacket or centroid.

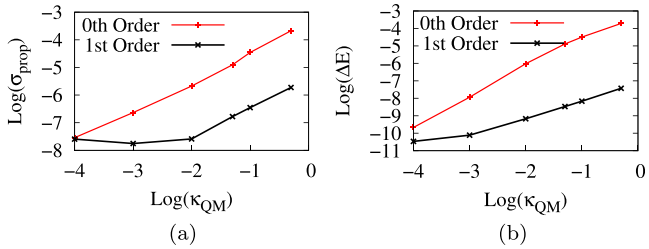

Figure 1. We present the logarithm of the (a) propagation error (eq 23) for the quantum centroid and (b) the root-mean-square deviation for the total energy in Hartree vs the logarithm of κ_{QM} (in atomic units). The red curve corresponds to the 0th-order scheme, whereas the black curve is the first-order scheme. The system was propagated for 1 ps with a time-step of 0.05 fs.

As expected, there is a clear dependence of the error on coupling strength. It is also clear that the first-order method is several orders of magnitude more accurate than the zeroth-order method across all values of coupling strengths. The same trend is seen in Figure 1b, where the energy conservation is shown as a function of κ_{QM}. The first-order method maintains good energy conservation over 1 ps at all values of κ_{QM} and has error orders of magnitude less than the original scheme. Furthermore, Figure 2a clearly shows that the first-order

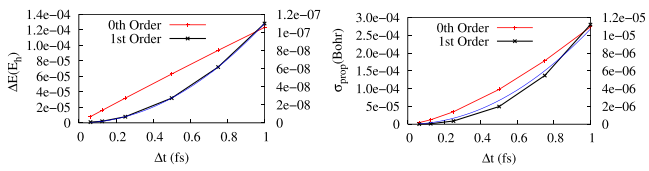

Figure 2. We present (a) the root-mean-square deviation in the total energy (ΔE), and (b) the propagation error [eq 23] for the quantum centroid as a function of integration time step [Δt] in fs. The red curve and left y-axis corresponds to the 0th-order scheme whereas the black curve and the right y-axis is the first-order scheme. The system was propagated for 1 ps, and the blue lines represent a quadratic function of the form $a\Delta t^2$.

method root-mean-square deviation in energy (ΔE) has a quadratic dependence on simulation time, whereas the zeroth-order method has a linear dependence. (A similar functional dependence is seen in Figure 2b, but the relationship is complicated by higher-order terms.) This quadratic relationship is expected[98] for third order integration schemes like velocity-Verlet and our Trotter-factorized quantum propagator. The linear relationship seen for the zeroth-order method does not conflict with the quadratic relationship published in ref 52, since only the quantum propagation was considered in that publication. Thus, approximating the time-dependence of the potential with a truncated Taylor expansion as outlined in the previous section results in a third-order, quantum-classical integration scheme.

In Figure 3, we present the time-evolution of the wavepacket density, centroid and classical particle for biased and unbiased trajectories. (The initial wavepacket is the same in both cases and this figure corresponds to κ_{QM} = 0.1 E_h/Bohr^2.) In Figure 3a, the green, blue and magenta contour lines, represent the wavepacket density for the case where no bias is used. Since the potential is harmonic, the wavepacket essentially does very little, and this is also seen from the wavepacket centroid, that is

https://doi.org/10.1021/acs.jpca.3c07385
J. Phys. Chem. A 2024, 128, 5386−5397

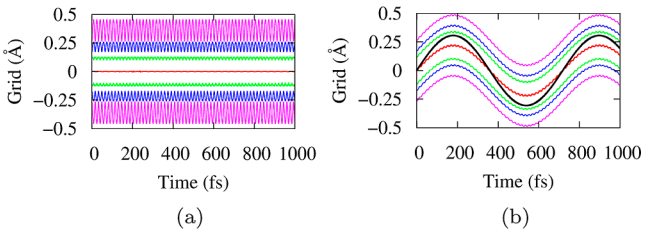

Figure 3. We present (a) the unbiased wavepacket density (with red, green, blue, and magenta contours) and (b) the biased wavepacket density, and the trajectory for the fictitious biasing degree of freedom (in black). The wavepacket density contour lines are 2.5×10^{-2} (green), 1×10^{-2} (blue) and 1×10^{-3} (magenta) and the red line is the wavepacket centroid for the trajectory.

red trace, which does not change with time. Figure 3b, shows the biased dynamics for the same harmonic potential in Figure 3a. Here, given the initial conditions on the bath particle (black trace), the wavepacket is pulled and oscillates on either sides of the potential well. Contour lines have the same magnitude for Figure 3a,b. Clearly, we sample higher energy regions with the biased scheme where the wavepacket oscillates about the minimum. This lays the groundwork for us to consider system 2 which now contains a barrier.

System 2: As stated previously, we also benchmarked this algorithm for a double-well potential (system 2). Since this potential contains a barrier, it is a reasonable starting point for probing this methodology in terms of the quantum mechanical sampling of reaction barriers and conformational transformations in future. The wavepacket grid is identical to that for system 1. The initial kinetic energy for the fictitious biasing degree of freedom is chosen to be 6.5 kcal/mol (that is below the barrier height) and the mass remains 350 amu as in the case of system 1. Again, as in system 1, the value of κ_{QM} is varied for identical reasons as presented in the discussion for system 1. We begin the simulation with the wavepacket localized in one of the wells (time zero slice in Figure 6a,b) and the initial wavepacket was thermalized according to

$$|\chi_0\rangle = \sum_i \exp[-\beta E_i]|\phi_i\rangle \tag{24}$$

where the eigenstates (eigenvalues) are $|\phi_i\rangle$ [(E_i) and β $(=1/k_B T)$ is the inverse temperature.

In Figure 4, we again note that the higher-order integration algorithm has better energy conservation across a wide range of

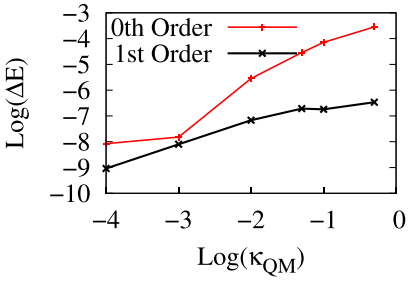

Figure 4. We present the logarithm of the root-mean-square of the total energy in Hartree versus the logarithm of κ_{QM} [in atomic units]. The red curve corresponds to the zeroth-order approximation in the Taylor series expansion in eq 18, whereas the black curve is the first order approximation. The system was propagated for 1 ps with a time-step of 0.05 fs.

coupling constant, κ_{QM}, values. In Figure 5, we also note that the algorithm retains its Δt^3 scaling in energy conservation.

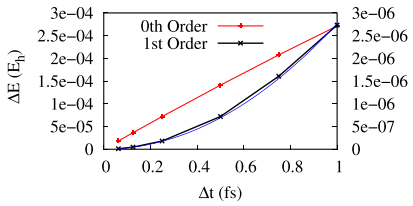

Figure 5. We show the root-mean-square deviation in the energy ΔE vs integration time-step (Δt) in fs. The red curve and left y-axis corresponds to the zeroth-order approximation in the Taylor series expansion in eq 18, whereas the black curve and the right y-axis is the first order approximation. The system was propagated for 1 ps with a time-step of 0.05 fs. The quadratic scaling of the first order approach is emphasized through the quadratic blue curve.

In Figure 6 we present the trajectories for the wavepacket density, its centroid and the fictitious biasing degree of

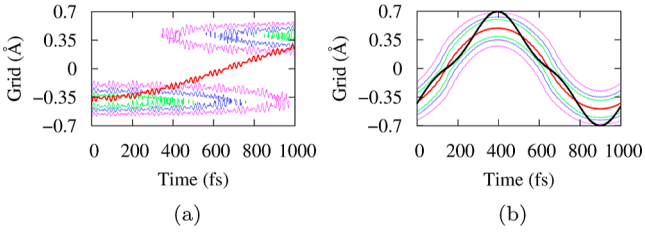

Figure 6. We present trajectories for (a) the unbiased wavepacket density and centroid trajectory and (b) the biased wavepacket density, centroid, and fictitious degree of freedom. The wavepacket density contours are shown at 2.5×10^{-2} (green), 1×10^{-2} (blue) and 1×10^{-3} (magenta) in (a), and 4×10^{-2} (green), 2.5×10^{-2} (blue) and 1×10^{-2} (magenta) in (b). In both cases, the red trace represents is the wavepacket centroid trajectory. In (b) the black trace depicts the trajectory for the fictitious biasing degree of freedom.

freedom. (This figure corresponds to $\kappa_{QM} = 0.1$ E_h/Bohr^2.) Figure 6a is the unbiased dynamics and can be understood as follows: As noted above, the system is initially localized and stable on one side of the barrier as indicated by the relative localization of the wavepacket near the time $t = 0$ slice. The wavepacket is highly oscillatory, which is expected, since contributions from high-energy eigenstates are required to enforce this localization. At about 400 fs, the second well begins to become accessible in Figure 6a (unbiased trajectory) because the quantum propagator allows for tunneling probabilities.[52,53,56,59,79,99] This accumulation is purely a quantum-mechanical (tunneling) effect. The centroid motion is shown in red in Figure 6a and accurately captures the wavepacket migration process.

The biased dynamics in Figure 6b drags the wavepacket over the barrier in a concerted fashion. For the biased dynamics the transition occurs earlier through the bath particle the dynamics for which is shown in black. One issue in this dynamics is that the wavepacket coherent oscillations in magenta and blue curves in Figure 6a are lost in Figure 6b, and it is this aspect that is critical to evaluate during choice of κ_{QM} as mentioned in response to the previous comment from the reviewer. The time-scale of this biased motion can be controlled through careful choice of κ_{QM}. As noted, in Figure 6 we present our results for $\kappa_{QM} = 0.1$ E_h/Bohr^2.

https://doi.org/10.1021/acs.jpca.3c07385
J. Phys. Chem. A 2024, 128, 5386−5397

4.2. Biased Classical Ab Initio Dynamics on the Phenol Amine System. In this section we study the phenol-trimethyl-amine, PhOH-N $(CH_3)_3$, which is considered a model proton transfer system (see Figure 7), using the classical

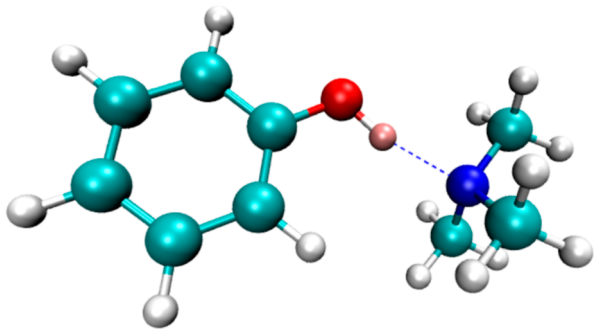

Figure 7. PhOH-N $(CH_3)_3$ system for biased classical ab initio dynamics benchmark. The transferring hydrogen atom is highlighted in pink, the donor-oxygen is in red, and acceptor nitrogen is in blue.

description of rare events introduced above. Such systems have been thought to be prototypical for condensed phase proton transfer[46] and involve critical quantum nuclear effects.[52,56,100] The delocalized electrons in the phenol ring and the associated polarizability of the amino group may stabilize the loss of the proton from the phenol group, facilitated by the surrounding polarizable electronic environment. The electronic structure for the system is treated here using B3LYP. The phenol-trimethylamine system has been previously studied[46] in a methanol solvent, however, solvent molecules are excluded from the current study, to simplify the problem. The time scale for the proton-transfer from the donor-oxygen to acceptor-nitrogen is hindered by the large potential barrier in the gas phase of ≈25 kcal/mol; furthermore, the product is an unstable zwitterion in the gas-phase thus providing a test for the current algorithm where the system is driven out of equilibrium into an unstable geometry, in a conservative fashion. Additionally, it is critical in such cases that the transformation be done in an effective and efficient way, while allowing suitable sampling of vibrational modes that remain orthogonal to the degrees of freedom actively involved in the transformation. Thus, the time-scale of transfer is critical.

As for the quantum nuclear systems mentioned above, here, we have tethered a fictitious particle to the shared hydrogen with a force constant of 0.1 E_h/Bohr^2 and performed the dynamics with both BOMD and ADMP performed at B3LYP/6-31+G(d,p). The choice of mass for the fictitious degrees of freedom was derived from the fact that the largest reduced mass of the normal modes is ≈7 amu, and we needed the fictitious degree of freedom to be well separated from the time scale of the other molecular vibrations.

Table 1 shows the energy conservation data for are simulations. The total energy (real plus fictitious) is conserved to within micro-Hartrees over picosecond length trajectories. Figure 8 displays the time-evolution of the reduced reaction coordinate, $(R_{OH} - R_{NH})/R_{ON}$. As can be seen, the rare-events sampling occurs more rapidly for the biased trajectories, while the unbiased trajectory oscillates and remains close to the initial configuration. We also note that fictitious bath degrees of freedom with greater masses allow for a lengthier sampling of the all degrees of freedom involved in the process, whereas the lighter fictitious particle eventually causes the cluster to

Table 1. Energy Conservation Summary

	$\tilde{M}^a$ (amu)	time (ps)	temp^b (K)	fictitious^c kinetic energy (kcal/mol)	ΔE^d (E_h)
BOMD	700	3.5	234.7	4.6	2.35×10^{-5}
	70	1.9	219.2	20.8	1.06×10^{-5}
ADMP	700	3.6	224.5	4.6	6.20×10^{-5}
	70	1.3	213	20.8	2.43×10^{-5}

^{a}The mass of the fictitious degree of freedom. ^{b}The temperature is calculated from the kinetic energy of the system. ^{c}This refers to the initial kinetic energy of the fictitious particle, not the kinetic energy of the density matrix in the ADMP trajectories. $^d\Delta E$ represents the standard deviation of the total energy (nuclear kinetic energy plus fictitious electronic kinetic energy plus potential energy) of the system during the simulation.

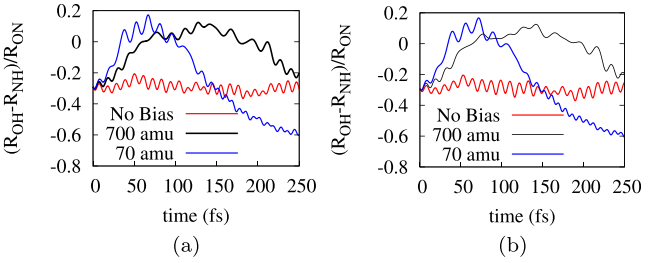

Figure 8. Reduced dimensional reaction coordinate, $(R_{OH} - R_{NH})/R_{ON}$ as a function of time. (a) BOMD results. (b) ADMP results. Both formalisms (ADMP and BOMD) effectively steer the shared hydrogen atom toward the nitrogen acceptor.

completely dissociate. This occurs since (a) there is no stable well on the acceptor side and (b) the cluster is bound by a weak, long-range hydrogen bond and the kinetic energy of the system is much greater than the stabilization of this well. To sample the acceptor side moiety completely, one needs to damp the kinetic energy of the fictitious particle smoothly. This was not considered as part of the current study, since the goal was to demonstrate a technique that samples rare events to probe the dynamical coupling that occurs during the process of such dynamics.

5. CONCLUDING REMARKS

In this paper, we proposed a scheme to allow both classical AIMD and quantum wavepacket dynamics to sample rare events on an accelerated time-scale. We accomplish this by introducing fictitious degrees of freedom that are bound to the molecular Hamiltonian. In essence then, these fictitious degrees of freedom steer the molecular dynamics over potential barriers in a reduced time-scale. The classical version of this approach was demonstrated on the PhOH-N $(CH_3)_3$ system for both Born−Oppenheimer and extended Lagrangian AIMD schemes. Here, a fictitious nuclear degree of freedom is introduced that allows one to quickly traverse the surface that connects the reactant and product states of this proton-coupled electron transfer process. Future studies will also use the theory developed here to allow the sampling of electronically rare events, that is, electronic structures that are no immediately accessible.

We also demonstrated the efficacy of this approach for quantum wavepacket dynamics, through an integration scheme wherein the implicit time-dependence of the potential energy surface, resulting from the introduction of a biasing nuclear degree of freedom is accounted for. This improves the overall

https://doi.org/10.1021/acs.jpca.3c07385
J. Phys. Chem. A 2024, 128, 5386−5397

scaling of errors of the quantum-classical integration from Δt^2 to Δt^3 for the strongly coupled system/biasing-bath problem studied here. This methodology will in future be generalized to account for coupling between classical and quantum nuclear degrees of freedom.

APPENDIX

Appendix A: Conservative Nature of eq 2

To probe the conservative nature of the Hamiltonian in eq 2, we first introduce the conjugate Lagrangian, given by the Legendre transform[77] of the Hamiltonian

$$\mathcal{L}_{SB} = \mathrm{Tr}(\mathcal{W}^{T}\mathbf{W}) + \mathrm{Tr}(\tilde{\mathcal{W}}^{T}\tilde{\mathbf{W}}) + \mathrm{Tr}(\mathcal{V}^{T}\mathbf{V}) + \mathrm{Tr}(\tilde{\mathcal{V}}^{T}\tilde{\mathbf{V}}) - \mathcal{H}_{SB} \tag{A1}$$

where $\mathcal{W}$, $\widetilde{\mathcal{W}}$, $\mathcal{V}$, and $\tilde{\mathcal{V}}$ are the conjugate momenta for $\mathbf{P}$, $\tilde{\mathbf{P}}$, $\mathbf{R}$, and $\tilde{\mathbf{R}}$, respectively, and are given by

$$\mathcal{W} = \frac{\partial \mathcal{L}_{SB}}{\partial \mathbf{W}} = \mu^{1/2}\mathbf{W}\mu^{1/2} \tag{A2}$$

$$\tilde{\mathcal{W}} = \frac{\partial \mathcal{L}_{SB}}{\partial \tilde{\mathbf{W}}} = \tilde{\mu}^{1/2}\tilde{\mathbf{W}}\tilde{\mu}^{1/2} \tag{A3}$$

$$\mathcal{V} = \frac{\partial \mathcal{L}}{\partial \mathbf{V}} = \mathbf{M}\mathbf{V} \tag{A4}$$

and

$$\tilde{\mathcal{V}} = \frac{\partial \mathcal{L}}{\partial \tilde{\mathbf{V}}} = \tilde{\mathbf{M}}\tilde{\mathbf{V}} \tag{A5}$$

Given these, the total derivative of $\mathcal{H}_{SB}$ with time is

$$\frac{d\mathcal{H}_{SB}}{dt} = \mathrm{Tr}\left[\left(\frac{\partial \mathcal{H}_{SB}}{\partial \mathbf{P}}\frac{d\mathbf{P}}{dt} + \frac{\partial \mathcal{H}_{SB}}{\partial \mathcal{W}}\frac{d\mathcal{W}}{dt}\right) + \left(\frac{\partial \mathcal{H}_{SB}}{\partial \mathbf{R}}\frac{d\mathbf{R}}{dt} + \frac{\partial \mathcal{H}_{SB}}{\partial \mathcal{V}}\frac{d\mathcal{V}}{dt}\right) + \left(\frac{\partial \mathcal{H}_{SB}}{\partial \tilde{\mathbf{R}}}\frac{d\tilde{\mathbf{R}}}{dt} + \frac{\partial \mathcal{H}_{SB}}{\partial \tilde{\mathcal{V}}}\frac{d\tilde{\mathcal{V}}}{dt}\right) + \left(\frac{\partial \mathcal{H}_{SB}}{\partial \tilde{\mathbf{P}}}\frac{d\tilde{\mathbf{P}}}{dt} + \frac{\partial \mathcal{H}_{SB}}{\partial \tilde{\mathcal{W}}}\frac{d\tilde{\mathcal{W}}}{dt}\right)\right] \tag{A6}$$

We next show that each of the terms inside brackets $(\cdots)$ is identically zero. For example, consider the first term

$$\left(\frac{\partial \mathcal{H}_{SB}}{\partial \mathbf{P}}\frac{d\mathbf{P}}{dt} + \frac{\partial \mathcal{H}_{SB}}{\partial \mathcal{W}}\frac{d\mathcal{W}}{dt}\right) \tag{A7}$$

Since the Hamiltonian in eq 2, governs the dynamics of $\{\mathbf{P},\mathbf{W},\mathbf{R},\mathbf{V}\}$ and bath variables, $\{\tilde{\mathbf{P}}, \tilde{\mathbf{W}}, \tilde{\mathbf{R}}, \tilde{\mathbf{V}}\}$, the quantity, $\frac{\partial \mathcal{H}_{SB}}{\partial \mathbf{P}}$ is the negative of a force acting on the classical variable $\mathbf{P}$, which describes the density matrix of the systems, and is equal to the rate of change of its momentum, $\frac{d\mathcal{W}}{dt}$. Thus

$$-\frac{\partial \mathcal{H}_{SB}}{\partial \mathbf{P}} = \frac{d\mathcal{W}}{dt} \tag{A8}$$

yields the equation of motion for $\mathbf{P}$. Additionally, using eq A1

$$\frac{\partial \mathcal{H}_{SB}}{\partial \mathcal{W}} = \mathbf{W} = \frac{d\mathbf{P}}{dt} \tag{A9}$$

and thus

$$\left(\frac{\partial \mathcal{H}_{SB}}{\partial \mathbf{P}}\frac{d\mathbf{P}}{dt} + \frac{\partial \mathcal{H}_{SB}}{\partial \mathcal{W}}\frac{d\mathcal{W}}{dt}\right) = 0 \tag{A10}$$

We can similarly prove that all four $(\cdots)$ bracketed terms, in Eq. are independently zero and

$$-\frac{\partial \mathcal{H}_{SB}}{\partial \tilde{\mathbf{P}}} = \frac{d\tilde{\mathcal{W}}}{dt} \tag{A11}$$

$$-\frac{\partial \mathcal{H}_{SB}}{\partial \mathbf{R}} = \frac{d\mathcal{R}}{dt} \tag{A12}$$

and

$$-\frac{\partial \mathcal{H}_{SB}}{\partial \tilde{\mathbf{R}}} = \frac{d\tilde{\mathcal{R}}}{dt} \tag{A13}$$

provide equations of motions for the respective variables. Together, along with the definitions for velocities as in eq B4, we arrive at

$$\frac{d\mathcal{H}_{SB}}{dt} = 0 \tag{A14}$$

This proves that the Hamiltonian in eq 2 is conservative and also provides the needed conduit to derive equations of motions.

Appendix B: Further Analysis of eqs 2 and AA1

The approach in this paper is along the lines of steered molecular dynamics[24,25] for classical force-field based molecular dynamics studies. The approach in this paper implements this scheme for classical AIMD and quantum AIMD. Ensemble properties for steered MD methods have been extensively discussed in the literature. As noted in eqs 1 and 2, we may partition the Hamiltonian in eq 2 as a system-bath Hamiltonian

$$\mathcal{H}_{SB} = \mathcal{H}_{S} + \mathcal{H}_{bath} \tag{B1}$$

Here $\mathcal{H}_{S}$ is defined in eq 1, and

$$\mathcal{H}_{bath} = \frac{1}{2}\mathrm{Tr}[\tilde{\mathbf{V}}^{T}\tilde{\mathbf{M}}\tilde{\mathbf{V}}] + \frac{1}{2}\mathrm{Tr}([\tilde{\mu}^{1/4}\tilde{\mathbf{W}}\tilde{\mu}^{1/4}]^2) + \mathrm{Tr}[\mathbf{\Lambda}_{\tilde{\mathbf{P}}}(\tilde{\mathbf{P}}\tilde{\mathbf{P}} - \tilde{\mathbf{P}})] + \eta(\mathbf{R}, \tilde{\mathbf{R}}, \mathbf{P}, \tilde{\mathbf{P}}; \kappa_{\mathbf{R}}, \kappa_{\mathbf{P}}) \tag{B2}$$

with

$$\eta(\mathbf{R}, \tilde{\mathbf{R}}, \mathbf{P}, \tilde{\mathbf{P}}; \kappa_{\mathbf{R}}, \kappa_{\mathbf{P}}) = \frac{1}{2}\mathrm{Tr}[(\mathbf{R} - \tilde{\mathbf{R}})^{T}\kappa_{\mathbf{R}}(\mathbf{R} - \tilde{\mathbf{R}})] + \frac{1}{2}\mathrm{Tr}[(\mathbf{P} - \tilde{\mathbf{P}})^{T}\kappa_{\mathbf{P}}(\mathbf{P} - \tilde{\mathbf{P}})] \tag{B3}$$

The goal is to choose $\eta(\mathbf{R}, \tilde{\mathbf{R}}, \mathbf{P}, \tilde{\mathbf{P}}; \kappa_{\mathbf{R}}, \kappa_{\mathbf{P}})$ to couple the degrees of freedom in $\{\mathbf{P},\mathbf{W},\mathbf{R},\mathbf{V}\}$ with $\{\tilde{\mathbf{P}}, \tilde{\mathbf{W}}, \tilde{\mathbf{R}}, \tilde{\mathbf{V}}\}$, to nudge the dynamics in the direction of the rare event in question.

In Section 2, we discussed the conservative nature of $\mathcal{H}_{SB}$. Thus, bounds to fluctuations in $\mathcal{H}_{S}$ and $\mathcal{H}_{bath}$ can also be established as follows.

https://doi.org/10.1021/acs.jpca.3c07385
J. Phys. Chem. A 2024, 128, 5386−5397

$$\frac{d\mathcal{H}_{bath}}{dt} = -\frac{d\mathcal{H}_S}{dt} = \mathrm{Tr}\left[\frac{\partial\mathcal{H}_{bath}}{\partial\mathbf{R}}\frac{d\mathbf{R}}{dt} + \frac{\partial\mathcal{H}_{bath}}{\partial\mathbf{P}}\frac{d\mathbf{P}}{dt} + \frac{\partial\mathcal{H}_{bath}}{\partial\tilde{\mathbf{R}}}\frac{d\tilde{\mathbf{R}}}{dt} + \frac{\partial\mathcal{H}_{bath}}{\partial\tilde{\mathbf{P}}}\frac{d\tilde{\mathbf{P}}}{dt} + \frac{\partial\mathcal{H}_{bath}}{\partial\tilde{\mathcal{V}}}\frac{\partial\mathcal{H}_{bath}}{\partial\tilde{\mathbf{W}}} - \frac{d\tilde{\mathbf{W}}}{dt}\right] \quad \text{(B4)}$$

where $\tilde{\mathcal{V}}$ and $\tilde{\mathcal{W}}$ are defined in eqs A5 and AA3. Since $\mathcal{H}_S$ is independent of $\{\tilde{\mathbf{P}}, \tilde{\mathbf{W}}, \tilde{\mathbf{R}}, \tilde{\mathbf{V}}\}$, it follows from the discussion in Appendix A, the sum of the last four terms on the right side of eq B4 is identically zero. Thus

$$\frac{d\mathcal{H}_{bath}}{dt} = \left(\frac{1}{2}(\mathbf{R}-\tilde{\mathbf{R}})^{\mathbf{T}}\kappa_{\mathbf{R}} - \frac{1}{2}\kappa_{\mathbf{R}}(\mathbf{R}-\tilde{\mathbf{R}})\right)\mathbf{V} + \left(\frac{1}{2}(\mathbf{P}-\tilde{\mathbf{P}})^{\mathbf{T}}\kappa_{\mathbf{P}} + \frac{1}{2}\kappa_{\mathbf{P}}(\mathbf{P}-\tilde{\mathbf{P}})\right)\mathbf{W} = \mathrm{Tr}\left[\frac{\partial\eta}{\partial\mathbf{R}}\mathbf{V} + \frac{\partial\eta}{\partial\mathbf{P}}\mathbf{W}\right] \quad \text{(B5)}$$

Thus, the fluctuations $\mathcal{H}_{bath}$ are dictated by fluctuations in the constraint term, and by the system velocities.

Dynamics trajectories constructed using eqs 6−9 may yield ensemble averages where the phase space is weighted according to the quantity $[\exp(-\beta\mathcal{H}_{SB})/Q_{\mathcal{H}_{SB}}]$. Here $Q_{\mathcal{H}_{SB}}$ is the partition function constructed from $\mathcal{H}_{SB}$. To obtain observables corresponding to $\mathcal{H}_S$, we write the ensemble average, we have

$$\langle A\rangle_{\mathcal{H}_S} \equiv \frac{\int d\Gamma_S A\exp(-\beta\mathcal{H}_S)}{\int d\Gamma_S\exp(-\beta\mathcal{H}_S)} = \frac{\int d\Gamma_S A\exp(+\beta\mathcal{H}_{bath})\exp(-\beta\mathcal{H}_{SB})}{\int d\Gamma_S\exp(+\beta\mathcal{H}_{bath})\exp(-\beta\mathcal{H}_{SB})} = \frac{\langle A\exp(+\beta\eta)\rangle'_{\mathcal{H}_{SB}}}{\langle\exp(+\beta\eta)\rangle'_{\mathcal{H}_{SB}}} \quad \text{(B6)}$$

where Γ_S includes the position and momenta from $\mathcal{H}_S$. As per the above equation, one needs to obtain averages for the quantity, $[A\exp(+\beta\eta)]$, and also monitor $\exp(+\beta\eta)$ during dynamics, where the latter provides the appropriate normalization (denominator above). The primes in the last equation above indicate that while the ensemble averages are constructed from the dynamic given by $\mathcal{H}_{SB}$, the integration is over the phase space of $\mathcal{H}_S$ and not $\mathcal{H}_{SB}$. Sampling issues that arise from such formalism are discussed in refs 21 and 24.

AUTHOR INFORMATION

Corresponding Author

Srinivasan S. Iyengar − *Department of Chemistry, Department of Physics, and the Indiana University Quantum Science and Engineering Center (IU-QSEC), Indiana University, Bloomington 47405 Indiana, United States;* orcid.org/0000-0001-6526-2907; Email: iyengar@indiana.edu

Authors

H. Bernhard Schlegel − *Department of Chemistry, Wayne State University, Detroit 48202 Michigan, United States;* orcid.org/0000-0001-7114-2821

Isaiah Sumner − *Department of Chemistry and Biochemistry, James Madison University, Harrisonburg 22807 Virginia, United States;* orcid.org/0000-0002-1422-5476

Junjie Li − *Texas Advanced Computing Center, The University of Texas at Austin, Austin 78758 Texas, United States*

Complete contact information is available at: https://pubs.acs.org/10.1021/acs.jpca.3c07385

Notes

The authors declare no competing financial interest.

ACKNOWLEDGMENTS

This research was supported by the National Science Foundation grant CHE-2102610 to S.S.I. and CHE-1856437 to H.B.S. The computational facilities at Indiana University are duly acknowledged and acknowledgment is due in part to the Lilly Endowment, Inc., for their support of the BigRed computing facility at Indiana University. This work was also supported in part by Shared University Research grants from IBM, Inc., to Indiana University, which supports the Scholarly Data Archives.

REFERENCES

(1) Wang, I. S. Y.; Karplus, M. Dyanmics of organic reactions. *J. Am. Chem. Soc.* **1973**, *95*, 8160−8164.

(2) Leforestier, C. Classical Trajectories Using the Full Ab Initio Potential Energy Surface $H^- + CH_4 \rightarrow CH_4 + H^-$. *J. Chem. Phys.* **1978**, *68*, 4406−4410.

(3) Car, R.; Parrinello, M. Unified Approach for Molecular Dynamics and Density-Functional Theory. *Phys. Rev. Lett.* **1985**, *55*, 2471−2474.

(4) Helgaker, T.; Uggerud, E.; Jensen, H. J. A. Integration of the Classical Equations of Motion on Ab Initio Molecular Potential Energy Surfaces Using Gradients and Hessians: Application to Translational Energy Release upon Fragmentation. *Chem. Phys. Lett.* **1990**, *173*, 145−150.

(5) Chen, W.; Hase, W. L.; Schlegel, H. B. Ab initio classical trajectory study of H2CO→H2+CO dissociation. *Chem. Phys. Lett.* **1994**, *228*, 436−442.

(6) Bolton, K.; Hase, W. L.; Peslherbe, G. H. In Modern Methods for Multidimensional Dynamics Computation in Chemistry. *Chapter Direct Dynamics of Reactive Systems*; Thompson, D. L., Ed.; World Scientific: Singapore, 1998; p 143.

(7) Schlegel, H. B.; Millam, J. M.; Iyengar, S. S.; Voth, G. A.; Daniels, A. D.; Scuseria, G. E.; Frisch, M. J. Ab Initio Molecular Dynamics: Propagating the Density Matrix with Gaussian Orbitals. *J. Chem. Phys.* **2001**, *114*, 9758−9763.

(8) Iyengar, S. S.; Schlegel, H. B.; Millam, J. M.; A Voth, G.; Scuseria, G. E.; Frisch, M. J. Ab Initio Molecular Dynamics: Propagating the Density Matrix with Gaussian Orbitals. II. Generalizations Based on Mass-Weighting, Idempotency, Energy Conservation and Choice of Initial Conditions. *J. Chem. Phys.* **2001**, *115*, 10291−10302.

(9) Iyengar, S. S.; Schlegel, H. B.; Voth, G. A.; Millam, J. M.; Scuseria, G. E.; Frisch, M. J. Ab Initio Molecular Dynamics: Propagating the Density Matrix with Gaussian Orbitals. IV. Formal Analysis of the Deviations from Born-Oppenheimer Dynamics. *Isr. J. Chem.* **2002**, *42*, 191−202.

(10) Benkovic, S. J.; Hammes-Schiffer, S. Enzyme Motions Inside and Out. *Science* **2006**, *312*, 208−209.

(11) Bolhuis, P. G.; Dellago, C.; Chandler, D.; Geissler, P. *Annu. Rev. Phys. Chem.* **2002**, *59*, 291.

(12) Elber, R.; Karplus, M. a Method for Determining Reaction Paths in Large Molecules: Application to Myoglobin. *Chem. Phys. Lett.* **1987**, *139*, 375−380.
(13) Elber, R.; Ghosh, A.; Cardenas, A. Bridging the Time Scales: Molecular Simulations for the Next Decade. *Chapter The Stochastic Difference Equation as a tool to compute long time dynamics*; Nielaba, P., Mareschal, M., Ciccotti, G., Eds.; Springer Verlag: Berlin, 2002; p 335.
(14) Elber, R.; Ghosh, A.; Cardenas, A. Long Time Dynamics of Complex Systems. *Acc. Chem. Res.* **2002**, *35*, 396−403.
(15) Gillilan, R. E.; Wilson, K. R. Shadowing, rare events, and rubber bands. A variational Verlet algorithm for molecular dynamics. *J. Chem. Phys.* **1992**, *97*, 1757−1772.
(16) Jarzynski, C. Equalities and Inequalities: Irreversibility and the Second Law of Thermodynamics at the Nanoscale. *Annu. Rev. Condens. Matter Phys.* **2011**, *2*, 329−351.
(17) Carter, E. A.; Ciccotti, G.; Hynes, J. T.; Kapral, R. Constrained Reaction Coordinate Dynamics for the Simulation of Rare Events. *Chem. Rev. Lett.* **1989**, *156*, 472−477.
(18) Ensing, B.; Laio, A.; Parrinello, M.; Klein, M. L. a Recipe for the Computation of the Free Energy Barrier and the Lowest Free Energy Path of Concerted Reactions. *J. Phys. Chem. B* **2005**, *109*, 6676−6687.
(19) Barducci, A.; Bonomi, M.; Parrinello, M. Metadynamics. *Wiley Interdiscip. Rev. Comput. Mol. Sci.* **2011**, *1*, 826−843.
(20) Maragliano, L.; Vanden-Eijnden, E. a Temperature Accelerated Method for Sampling Free Energy and Determining Reaction Pathways in Rare Events Simulations. *Chem. Phys. Lett.* **2006**, *426*, 168−175.
(21) MacFadyen, J.; Andricioaei, I. a Skewed-Momenta Method to Efficiently Generate Conformational-Transition Trajectories. *J. Chem. Phys.* **2005**, *123*, 074107.
(22) Passerone, D.; Parrinello, M. Action-Derived Molecular Dynamics in the Study of Rare Events. *Phys. Rev. Lett.* **2001**, *87*, 108302.
(23) Passerone, D.; Ceccarelli, M.; Parrinello, M. a Concerted Variational Strategy for Investigating Rare Events. *J. Chem. Phys.* **2003**, *118*, 2025−2032.
(24) Park, S.; Schulten, K. Calculating Potentials of Mean Force from Steered Molecular Dynamics Simulations. *J. Chem. Phys.* **2004**, *120*, 5946−5961.
(25) Izrailev, S.; Stepaniants, S.; Balsera, M.; Oono, Y.; Schulten, K. Molecular dynamics study of unbinding of the avidin-biotin complex. *Biophys. J.* **1997**, *72*, 1568−1581.
(26) Voter, A. F. a Method for Accelerating the Molecular Dynamics Simulation of Infrequent Events. *J. Chem. Phys.* **1997**, *106*, 4665−4677.
(27) Hammes-Schiffer, S.; Tully, J. Nonadiabatic Transition-State Theory and Multiple Potential-Energy Surface Molecular-Dynamics of Infrequent Events. *J. Chem. Phys.* **1995**, *103*, 8528−8537.
(28) Wang, L.-P.; Titov, A.; McGibbon, R.; Liu, F.; Pande, V. S.; Martínez, T. J. Discovering chemistry with an ab initio nanoreactor. *Nat. Chem.* **2014**, *6*, 1044−1048.
(29) Chang, A. M.; Meisner, J.; Xu, R.; Martínez, T. J. Efficient Acceleration of Reaction Discovery in the Ab Initio Nanoreactor: Phenyl Radical Oxidation Chemistry. *J. Phys. Chem. A* **2023**, *127*, 9580−9589.
(30) Kaledin, M.; Brown, A.; Kaledin, A. L.; Bowman, J. M. Normal Mode Analysis Using the Driven Molecular Dynamics Method. II. an Application to Biological Macromolecules. *J. Chem. Phys.* **2004**, *121*, 5646−5653.
(31) Ilan, B.; Tajkhorshid, E.; Schulten, K.; Voth, G. A. The Mechanism of Proton Exclusion in Aquaporin Channels. *Proteins: Struct., Funct., Bioinf.* **2004**, *55*, 223−228.
(32) Park, S.; Khalili-Araghi, F.; Tajkhorshid, E.; Schulten, K. Free Energy Calculation from Steered Molecular Dynamics Simulations Using Jarzynski's Equality. *J. Chem. Phys.* **2003**, *119*, 3559−3566.
(33) Phatak, P.; Sumner, I.; Iyengar, S. S. Gauging the Flexibility of the Active Site in Soybean Lipoxygenase-1 (SLO-1) Through an Atom-Centered Density Matrix Propagation (ADMP) Treatment That Facilitates the Sampling of Rare Events. *J. Phys. Chem. B* **2012**, *116*, 10145−10164.
(34) Phatak, P.; Venderley, J.; Debrota, J.; Li, J.; Iyengar, S. S. Active Site Dynamical Effects in the Hydrogen Transfer Rate-limiting Step in the Catalysis of Linoleic Acid by Soybean Lipoxygenase-1 (SLO-1): Primary and Secondary Isotope Contributions. *J. Phys. Chem. B* **2015**, *119*, 9532−9546.
(35) DeGregorio, N.; Iyengar, S. S. Challenges in constructing accurate methods for hydrogen transfer reactions in large biological assemblies: rare events sampling for mechanistic discovery and tensor networks for quantum nuclear effects. *Faraday Discuss.* **2020**, *221*, 379−405.
(36) Henkelman, G.; Jonsson, H. Improved Tangent Estimate in the Nudged Elastic Band Method for Finding Minimum Energy Paths and Saddle Points. *J. Chem. Phys.* **2000**, *113*, 9978−9985.
(37) Abrams, J. B.; Tuckerman, M. E. Efficient and Direct Generation of Multidimensional Free Energy Surfaces via Adiabatic Dynamics without Coordinate Transformations. *J. Phys. Chem. B* **2008**, *112*, 15742−15757.
(38) So/rensen, M. R.; Voter, A. F. Temperature-Accelerated Dynamics for Simulation of Infrequent Events. *J. Chem. Phys.* **2000**, *112*, 9599−9606.
(39) Voter, A. F. Hyperdynamics: Accelerated Molecular Dynamics of Infrequent Events. *Phys. Rev. Lett.* **1997**, *78*, 3908−3911.
(40) Dellago, C.; Bolhuis, P. G.; Csajka, F. S.; Chandler, D. Transition Path Sampling and the Calculation of Rate Constants. *J. Chem. Phys.* **1998**, *108*, 1964−1977.
(41) Paci, E.; Karplus, M. Forced Unfolding of Fibronectin Type 3 Modules: An Analysis by Biased Molecular Dynamics Simulations. *J. Mol. Biol.* **1999**, *288*, 441−459.
(42) Andersen, H. C. Molecular Dynamics Simulations at Constant Pressure And/or Temperature. *J. Chem. Phys.* **1980**, *72*, 2384−2393.
(43) Parrinello, M.; Rahman, A. Crystal Structure and Pair Potentials: A Molecular-Dynamics Study. *Phys. Rev. Lett.* **1980**, *45*, 1196−1199.
(44) Nosé, S. A unified formulation of the constant temperature molecular dynamics methods. *J. Chem. Phys.* **1984**, *81*, 511−519.
(45) Hoover, W. G. Canonical Dynamics: Equilibrium Phase-Space Distributions. *Phys. Rev. A: At., Mol., Opt. Phys.* **1985**, *31*, 1695−1697.
(46) Hammes-Schiffer, S.; Tully, J. C. Proton Transfer in Solution: Molecular Dynamics with Quantum Transitions. *J. Chem. Phys.* **1994**, *101*, 4657−4667.
(47) Jarzynski, C. Nonequilibrium Equality for Free Energy Differences. *Phys. Rev. Lett.* **1997**, *78*, 2690−2693.
(48) Jarzynski, C. Equilibrium Free-Energy Differences from Nonequilibrium Measurements: A Master-Equation Approach. *Phys. Rev. E: Stat. Phys., Plasmas, Fluids, Relat. Interdiscip. Top.* **1997**, *56*, 5018−5035.
(49) Presse, S.; Silbey, R. Ordering of Limits in the Jarzynski Equality. *J. Chem. Phys.* **2006**, *124*, 054117.
(50) Presse, S.; Silbey, R. J. Memory Effects on the Convergence Properties of the Jarzynski Equality. *Phys. Rev. E: Stat. Phys., Plasmas, Fluids, Relat. Interdiscip. Top.* **2006**, *74*, 061105.
(51) Liphardt, J.; Dumont, S.; Smith, S.; Tinoco, I.; Bustamante, C. Equilibrium Information from Nonequilibrium Measurements in an Experimental Test of Jarzynski's Equality. *Science* **2002**, *296*, 1832−1835.
(52) Iyengar, S. S.; Jakowski, J. Quantum Wavepacket Ab Initio Molecular Dynamics: An Approach to Study Quantum Dynamics in Large Systems. *J. Chem. Phys.* **2005**, *122*, 114105.
(53) Iyengar, S. S. *Ab Initio* Dynamics with Wave-Packets and Density Matrices. *Theor. Chem. Accts.* **2006**, *116*, 326−337.
(54) Jakowski, J.; Sumner, I.; Iyengar, S. S. Computational improvements to quantum wave packet *ab initio* molecular dynamics using a potential-adapted, time-dependent deterministic sampling technique. *J. Chem. Theory Comput.* **2006**, *2*, 1203−1219.
(55) Sumner, I.; Iyengar, S. S. Quantum Wavepacket *Ab Initio* Molecular Dynamics: An Approach for Computing Dynamically

https://doi.org/10.1021/acs.jpca.3c07385
J. Phys. Chem. A 2024, 128, 5386−5397

Averaged Vibrational Spectra Including Critical Nuclear Quantum Effects. *J. Phys. Chem. A* **2007**, *111*, 10313−10324.
(56) Iyengar, S. S.; Sumner, I.; Jakowski, J. Hydrogen Tunneling in an Enzyme Active Site: A Quantum Wavepacket Dynamical Perspective. *J. Phys. Chem. B* **2008**, *112*, 7601−7613.
(57) Li, X.; Iyengar, S. S. Quantum Wavepacket *Ab Initio* Molecular Dynamics: Generalizations Using an Extended Lagrangian Treatment of Diabatic States Coupled Through Multi-Reference Electronic Structure. *J. Chem. Phys.* **2010**, *133*, 184105.
(58) Li, J.; Li, X.; Iyengar, S. S. Vibrational Properties of Hydrogen Bonded Systems Using the Multi-Reference Generalization to the "On-The-Fly" Electronic Structure Within Quantum Wavepacket *Ab Initio* Molecular Dynamics (QWAIMD). *J. Chem. Theory Comput.* **2014**, *10*, 2265−2280.
(59) Prociuk, A. H.; Iyengar, S. S. A Multi-Wavelet Treatment of the Quantum Subsystem in Quantum Wavepacket Ab-Initio Molecular Dynamics Through an Hierarchical Partitioning of Momentum Space. *J. Chem. Theory Comput.* **2014**, *10*, 2950−2963.
(60) Caldeira, A. O.; Leggett, A. J. Quantum tunnelling in a dissipative system. *Ann. Phys.* **1983**, *149*, 374−456.
(61) Leggett, A. J.; Chakravarty, S.; Dorsey, A. T.; Fisher, M. P. A.; Garg, A.; Zwerger, W. Dynamics of the dissipative two-state system. *Rev. Mod. Phys.* **1987**, *59*, 1−85.
(62) Schlegel, H. B.; Iyengar, S. S.; Li, X.; Millam, J. M.; Voth, G. A.; Scuseria, G. E.; Frisch, M. J. Ab Initio Molecular Dynamics: Propagating the Density Matrix with Gaussian Orbitals. III. Comparison with Born-Oppenheimer Dynamics. *J. Chem. Phys.* **2002**, *117*, 8694−8704.
(63) Iyengar, S. S.; Frisch, M. J. Effect of Time-Dependent Basis Functions and Their Superposition Error on Atom-Centered Density Matrix Propagation (ADMP): Connections to Wavelet Theory of Multi-Resolution Analysis. *J. Chem. Phys.* **2004**, *121*, 5061−5070.
(64) Rega, N.; Iyengar, S. S.; Voth, G. A.; Schlegel, H. B.; Vreven, T.; Frisch, M. J. Hybrid Ab-Initio/Empirical Molecular Dynamics: Combining the ONIOM Scheme with the Atom-Centered Density Matrix Propagation (ADMP) Approach. *J. Phys. Chem. B* **2004**, *108*, 4210−4220.
(65) Li, J.; Haycraft, C.; Iyengar, S. S. Hybrid, Extended Lagrangian − Born-Oppenheimer *Ab Initio* Molecular Dynamics using Fragment-Based Electronic Structure. *J. Chem. Theory Comput.* **2016**, *12*, 2493−2508.
(66) Li, J.; Iyengar, S. S. Ab initio Molecular Dynamics using Recursive, Spatially Separated, Overlapping Model Subsystems Mixed Within an ONIOM Based Fragmentation Energy Extrapolation Technique. *J. Chem. Theory Comput.* **2015**, *11*, 3978−3991.
(67) Haycraft, C.; Li, J.; Iyengar, S. S. Efficient On-the-fly" Born−Oppenheimer and Car−Parrinello−type Dynamics with coupled cluster accuracy through Fragment Based Electronic Structure. *J. Chem. Theory Comput.* **2017**, *13*, 21887−21901.
(68) Ricard, T. C.; Haycraft, C.; Iyengar, S. S. Adaptive, geometric networks for efficient coarse-grained *ab initio* molecular dynamics with post-Hartree-Fock accuracy. *J. Chem. Theory Comput.* **2018**, *14*, 2852−2866.
(69) Ricard, T. C.; Iyengar, S. S. Efficiently capturing weak interactions in *ab initio* molecular dynamics through "on-the-fly" basis set extrapolation. *J. Chem. Theory Comput.* **2018**, *14*, 5535−5552.
(70) Iyengar, S. S.; Schlegel, H. B.; Voth, G. A. Atom-Centered Density Matrix Propagation (ADMP): Generalizations Using Bohmian Mechanics. *J. Phys. Chem. A* **2003**, *107*, 7269−7277.
(71) Madelung, E. Quantentheorie in Hydrodynamischer Form. *Z. Phys.* **1927**, *40*, 322−326.
(72) de Broglie, L. *An Introduction to the Study of Wave Mechanics*; E. P. Dutton and Company, Inc.: New York, 1930.
(73) Bohm, D. A Suggested Interpretation of the Quantum Theory in Terms of "Hidden" Variables. I. *Phys. Rev.* **1952**, *85*, 166−179.
(74) *Bohmian Mechanics: An Appraisal*; Cushing, J. T., Fine, A., Goldstein, S., Eds.; Kluwer: Boston, 1996.
(75) Holland, P. R. *The Quantum Theory of Motion*; Cambridge: New York, 1993.
(76) Lopreore, C. L.; Wyatt, R. E. Quantum Wave Packet Dynamics with Trajectories. *Phys. Rev. Lett.* **1999**, *82*, 5190−5193.
(77) Goldstein, H.; Poole, C.; Safko, J. *Classical Mechanics*; Addison Wesley: San Francisco, 2002.
(78) Hammes-Schiffer, S.; Benkovic, S. J. Relating Protein Motion to Catalysis. *Annu. Rev. Biochem.* **2006**, *75*, 519−541.
(79) Sumner, I.; Iyengar, S. S. Combining Quantum Wavepacket *Ab Initio* Molecular Dynamics (QWAIMD) with QM/MM and QM/QM Techniques: Implementation Blending ONIOM and Empirical Valence Bond Theory. *J. Chem. Phys.* **2008**, *129*, 054109.
(80) Gerber, R. B.; Buch, V.; Ratner, M. A. Time-Dependent Self-Consistent Field Approximation for Intramolecular Energy Transfer. I. Formulation and Application to Dissociation of Van Der Waals Molecules. *J. Chem. Phys.* **1982**, *77*, 3022−3030.
(81) Bisseling, R. H.; Kosloff, R.; Gerber, R. B.; Ratner, M. A.; Gibson, L.; Cerjan, C. Exact Time-Dependent Quantum Mechanical Dissociation Dynamics of I_2He: Comparison of Exact Time-Dependent Quantum Calculation with the Quantum Time-Dependent Self-Consistent Field (TDSCF) Approximation. *J. Chem. Phys.* **1987**, *87*, 2760−2765.
(82) Makri, N.; Miller, W. H. Time-Dependent Self-Consistent Field (TDSCF) Approximation for a Reaction Coordinate Coupled to a Harmonic Bath—Single and Multiple Configuration Treatments. *J. Chem. Phys.* **1987**, *87*, 5781−5787.
(83) McCoy, A. B.; Gerber, R. B.; Ratner, M. A. A. Quantitative Approximation for the Quantum Dynamics of Hydrogen Transfer: Transition State Dynamics and Decay in $ClHCl^-$. *J. Chem. Phys.* **1994**, *101*, 1975−1987.
(84) Jasper, A. W.; Zhu, C.; Nangia, S.; Truhlar, D. G. Introductory Lecture: Nonadiabatic Effects in Chemical Dynamics. *Faraday Discuss.* **2004**, *127*, 1.
(85) Coker, D. F. *Computer Simulation in Chemical Physics*; Allen, M. P., Tildesley, D. J., Eds.; Kluwer Academic Publishers: Dordrecht, The Netherlands, 1993.
(86) Tully, J. C. Molecular Dynamics with Electronic Transitions. *J. Chem. Phys.* **1990**, *93*, 1061−1071.
(87) Martinez, T. J.; BenNun, M.; Ashkenazi, G. Classical/quantal Method for Multistate Dynamics: A Computational Study. *J. Chem. Phys.* **1996**, *104*, 2847−2856.
(88) Mead, C. A.; Truhlar, D. G. On the Determination of Born-Oppenheimer Nuclear Motion Wave Functions Including Complications Due to Conical Intersections and Identical Nuclei. *J. Chem. Phys.* **1979**, *70*, 2284−2296.
(89) Kuppermann, A. The Geometric Phase in Reaction Dynamics. In *Dynamics of Molecules and Chemical Reactions*; Wyatt, R. E., Zhang, J. Z. H., Eds.; Marcel Dekker Inc.: New York, NY, 1996; p 411.
(90) Yarkony, D. R. Diabolical Conical Intersections. *Rev. Mod. Phys.* **1996**, *68*, 985−1013.
(91) Wu, B.; He, X.; Liu, J. Nonadiabatic Field on Quantum Phase Space: A Century after Ehrenfest. *J. Phys. Chem. Lett.* **2024**, *15*, 644−658.
(92) Tully, J. C.; Preston, R. K. Trajectory surface hopping approach to nonadiabatic molecular collisions: the reaction of H^+ with D_2. *J. Chem. Phys.* **1971**, *55*, 562−572.
(93) Tully, J. C. Nonadiabatic molecular dynamics. *Int. J. Quantum Chem.* **1991**, *40*, 299−309.
(94) Tannor, D. J. *Introduction to Quantum Mechanics: A Time-Dependent Perspective*; University Science Books, 2007.
(95) Kohen, D.; Stillinger, F. H.; Tully, J. C. Model Studies of Nonadiabatic Dynamics. *J. Chem. Phys.* **1998**, *109*, 4713−4725.
(96) Golub, G. H.; Loan, C. F. V. *Matrix Computations*; The Johns Hopkins University Press: Baltimore, 1996.
(97) Iyengar, S. S.; Kouri, D. J.; Parker, G. A.; Hoffman, D. K. Estimating bounds on the highest and lowest eigenvalues of any matrix. *Theor. Chem. Acc.* **2000**, *103*, 507−517.
(98) Allen, M. P.; Tildesley, D. J. *Computer Simulation in Chemical Physics*; Springer Science & Business Media, 2012; Vol. 397.

https://doi.org/10.1021/acs.jpca.3c07385
J. Phys. Chem. A 2024, 128, 5386−5397

(99) Li, X.; Iyengar, S. S. Quantum Wavepacket Ab Initio Molecular Dynamics for Extended Systems. *J. Phys. Chem. A* **2011**, *115*, 6269−6284.
(100) Costentin, C.; Saveant, J.-M. Why Are Proton Transfers at Carbon Slow? Self-Exchange Reactions. *J. Am. Chem. Soc.* **2004**, *126*, 14787−14795.

https://doi.org/10.1021/acs.jpca.3c07385
J. Phys. Chem. A 2024, 128, 5386−5397